

Analysis of Unsteady Propeller Blade Forces by RANS

Vladimir Krasilnikov¹, Zhirong Zhang² and Fangwen Hong²

¹Norwegian Marine Technology Research Institute (MARINTEK), Trondheim, Norway

²China Ship Scientific Research Center (CSSRC), Wuxi, Jiangsu, China

ABSTRACT

The paper describes some of the authors' results with the numerical prediction of unsteady forces acting on propeller blades using a Reynolds Averaged Navier-Stokes (RANS) method. An automated mesh generation technique is proposed to be used with different types of marine propulsors, and it is presently applied to the analysis of open and podded propellers operating in oblique flow conditions. The paper presents recent validation results obtained with the method and illustrates the differences in forces experienced by a podded propeller operating in pulling and pushing modes.

Keywords

Podded propellers, Oblique flow, Unsteady forces, CFD, RANS.

1 INTRODUCTION

The propeller operating behind ship hull represents a source of periodical forces transmitted to the hull through the shafting system and water. These periodical forces result in additional unsteady loads on the shaft and cause vibration in the hull and ship systems. The propeller blade forces and moments of hydrodynamic nature form a substantial contribution to the total force balance. Apart from the vibration issues, the information about these forces is important for the blade strength analysis and, as far as CP propellers are concerned, for the design of blade pitching mechanism. Interaction between the hull and propeller, as well as between the components of propulsion system is the key factor to be accounted for in the prediction of periodical forces. Additional concerns arise for propellers operating in oblique flow conditions caused by shaft inclination or azimuthing angle of pod drives. For podded propellers, flow angle can reach very large values resulting in large amplitudes of blade forces during revolution.

The investigation in unsteady blade forces requires development of advanced experimental and numerical techniques. Experimental blade force measurements go back to 70-s when studies have been started on blade loads in oblique flows and simplified artificial wake fields. For example, in 1973, the tests done at KMW Marine Laboratories, Kristinehamn, Sweden for DNV included measurements of one blade thrust, torque, transverse force, bending moment and spindle moment on

a 4-bladed low skew propeller operating in oblique flow of 10 degrees, and behind wake screens providing V-shape axial wakes in the sectors of 10 and 90 degrees, as well as in the wake field obtained by superposition of oblique flow and V-shape axial wake (Ræstad, 2007). Single blade force measurements on a moderate skew propeller (DTMB propeller 4661) in oblique flows of 10, 20 and 30 deg were reported in (Boswell et al, 1981; 1984). The experimental data referred above have been used for the validation of potential propeller analysis codes by many authors. The well-known symmetric 3-bladed propeller DTMB4119 was tested in the 24-inch water tunnel behind harmonic wake screens with 3, 6, 9 and 12 cycles per revolution, and one blade thrust and torque were measured in (Jessup, 1990). Apart from blade force measurements, efforts have been put into studies on unsteady blade pressure distribution. The most well-known openly available results are represented by the model scale propeller DTMB4679 (Jessup, 1982) and the full scale propeller SEIUN-MARU HSP (Ukon, 1991). Both cases were used for the comparative validation of potential propeller analysis codes at the ITTC Propeller Workshop in 1998, and the results were summarized in (ITTC, 1998). Concerning podded propellers, a number of experimental studies were reported and used in experimental/numerical comparisons focusing on integral forces acting on the propeller and on the unit (Achkinadze et al, 2003), (Grygorowicz & Szantyr, 2004), (Heinke, 2004). The test results used in (Achkinadze et al, 2003) are part of the large matrix from the test program conducted in the towing tank at MARINTEK with the Pull/Push Azimuthing Thruster T14. It covers a wide range of operating conditions in terms of advance coefficient and heading angle. Those tests did not include, however, one blade force measurements. An original six-component blade dynamometer designed and manufactured at MARINTEK was used in a number of tests with the Pushing Azimuthing Thruster T98 equipped with both the open and ducted propellers, where the focus was made primarily on dynamic blade loads arising in seaway and due to ventilation (Koushan, 2006; 2007). An overview of numerical methods applied to the analysis of propellers operating in oblique flows is given (Krasilnikov & Sun, 2008) and (Koushan & Krasilnikov, 2008). Generally, when the problem is set to analyze a

propeller in oblique flow, viscous flow RANS methods are preferred to potential or viscous/potential hybrid calculations, when the flow angles are larger than 15-20 degrees. For podded propellers, the interaction between the propeller and housing is important. It is shown in (Koushan & Krasilnikov, 2008) that only RANS methods allow one to simulate naturally the complex flow around pod housing and predict asymmetry in characteristics of pushing propeller observed in the tests. Apart from the above reference, a limited number of unsteady RANS calculations with pod propulsors were presented focusing on scale effect on pod housing (Sanchez-Caja & Ory, 2003), optimization of housing outlines (Sanchez-Caja & Pylkkanen, 2004) and forces arising on podded units in oblique flows (Junglewitz & El Moctar, 2004), (Junglewitz et al, 2004).

RANS simulations of propeller in ship hull wakes are best performed in presence of ship hull. While there are known attempts to perform simulations in given wake field separated from ship hull, they have apparent limitations since in RANS, unlike potential flow methods, it is impossible to prescribe a desired wake field at the propeller location.

Generally, all aforementioned unsteady RANS simulations of propeller are to be done with sliding mesh technique to allow for time accurate flow solution. Quasi-steady approach based on the concept of “frozen rotor” can not provide adequate results in terms of single blade forces and pressure distributions. However, it can be employed to obtain initial conditions for time accurate unsteady analysis (Krasilnikov & Sun, 2008).

In the present paper, an unsteady RANS method with the original automated mesh generation technique is applied to the analysis of single propellers and podded propellers operating in oblique flow. Validation results are presented with respect to unsteady blade pressure distributions on the propeller DTMB4679 in oblique flow, propeller from the KMW tests in oblique flow, and propeller and unit forces on the MARINTEK Pull/Push Azimuthing Thruster T14. In the latter case, where the inflow on propeller is influenced, to significant degree, by the interaction between propeller and housing, single blade forces are analyzed and compared for the pulling and pushing propellers.

2 APPROACH

The RANS method used in this work employs a segregated solver of the commercial CFD code FLUENT and the original automated mesh generation techniques developed under a joint project between MARINTEK and China Ship Scientific Research Center (CSSRC) (Zhang and Hong, 2007), (Krasilnikov et al, 2007), (Krasilnikov & Sun, 2008). The meshing techniques are different for the cases of single propeller and podded propeller.

2.1 Meshing technique

For a single open propeller, the solution domain represents a cylinder with its inlet located at 4 propeller diameters upstream of propeller plane, and its outlet located at 6 propeller diameters downstream of propeller plane, and cylinder radius being equal to 4 propeller diameters. The whole computation domain is divided, in this case, into the six blocks. In the block surrounding

propeller, an unstructured grid of prismatic and tetrahedral cells is built. The wall cell size on the blade and hub surfaces is defined as $k_{MF} \cdot 0.005 \cdot D$, where D is the propeller diameter and k_{MF} is the mesh factor which regulates mesh fineness. At the outer faces of the propeller block, the cell size is equal to $3 \cdot k_{MF} \cdot 0.005 \cdot D$, and inside of the block the cell size increases linearly from blade and hub surfaces to the outer faces with the coefficient of 1.1. Structured meshes are built in the remaining blocks. In particular, in the blocks built upstream and downstream of propeller, the grids feature prismatic cells (wedges), and in the blocks of the outer domain the cells are hexahedral. The cell size at the faces of these blocks attached to the propeller block is $3 \cdot k_{MF} \cdot 0.005 \cdot D$, from where it increases linearly outward with the coefficient of 1.2. The use of single mesh factor k_{MF} allows for simple and efficient mesh refinement or coarsening. Both the enhanced and coarse wall treatment can be provided, but all simulations done in this work with open propellers have been performed with “coarse” wall treatment providing wall $Y^+ > 30$. An example of intentionally coarsened mesh around single propeller DTMB4679 is shown in Figure 1.

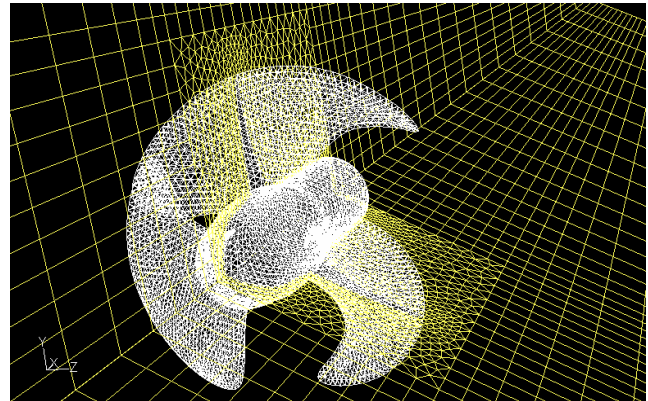


Figure 1. Example of mesh around single open propeller.

When a podded propeller is modeled, a cylindrical computation domain is built around the unit with the inlet located at 2.5 gondola lengths upstream of the gondola mid-section, outlet located at 5 gondola lengths downstream of the gondola mid-section, and the domain radius being equal to 3 gondola lengths. The domain is divided into the seven blocks. The blocks formed around propulsor are shown in Figure 2. They include the block containing rotating propeller and hub, the block containing middle part of the gondola with part of strut and bottom fin (if such is present in simulated arrangement), and the block containing end of the gondola opposite to propeller location. All blocks are meshed with tetrahedral cells, thus, resulting in a completely unstructured mesh. The mesh fineness in the blocks is controlled by the mesh factor and volume mesh size functions, similar to the case of single open propeller.

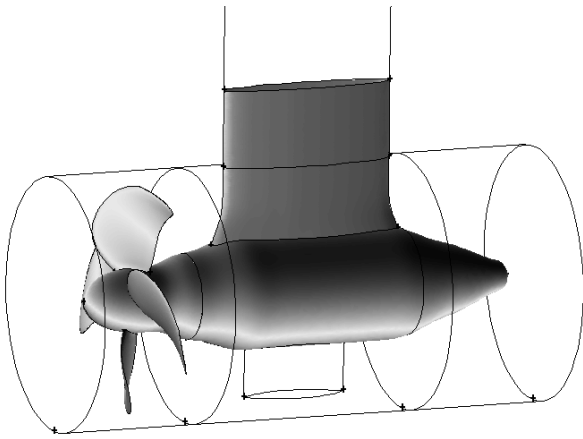


Figure 2. Mesh blocks around pulling podded propeller.

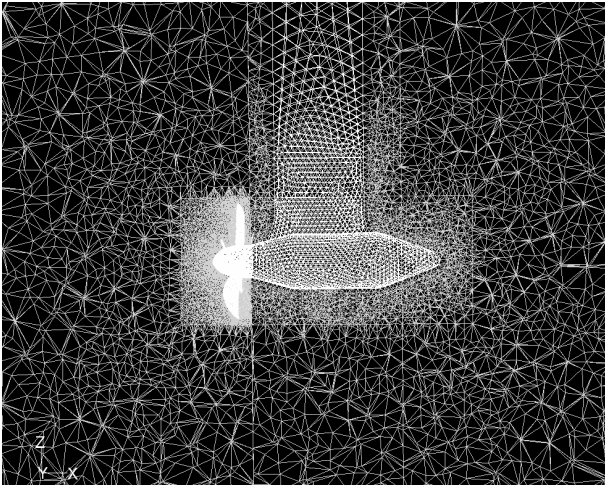


Figure 3. Volume mesh around a pulling azimuthing pod thruster.

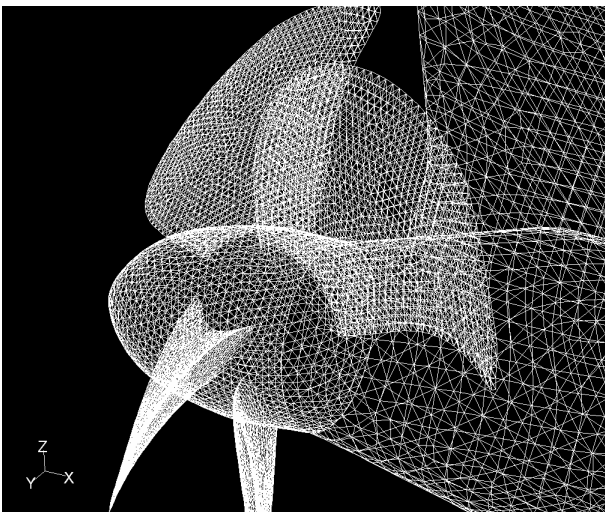


Figure 4. Fragment of surface mesh on propeller, hub and housing of a pulling azimuthing pod thruster.

Figures 3 and 4 illustrate some details of volume and surface meshes for the MARINTEK Pull/ Push Azimuting Thruster T14 used in the simulations in the present paper.

The interface sliding mesh technique is used in unsteady simulation. It requires two interface zones to be created at the adjacent boundaries of the rotating mesh block containing propeller and hub, and the stationary mesh block containing, for example, strut and middle part of the gondola. These interface zones are associated to form the grid interface along which the rotating mesh block will slide at the time-dependent stage of the solution. For the single propeller, it is, essentially, the same, except that unstructured mesh block around propeller slides with respect to outer structured mesh blocks. In the FLUENT solver, the faces of the adjacent mesh blocks do not require alignment on the grid interface, and the fluxes across the grid interface are computed using the faces obtained from the intersection of the interface zones, at each time step.

1.2 Turbulence model

The Shear Stress Transport (SST) $k-\omega$ turbulence model is employed to calculate Reynolds stresses in the RANS equations. The advantages of this model are seen in its ability to cope simultaneously with low Re (near-wall) and high Re (far-field) zones, and to predict more accurately non-equilibrium regions in boundary layer with adverse pressure gradients such as separation domains. The latter may be of particular importance when calculating propellers under off-design condition (for example, heavy loading, large off-design blade installation angles of CP propeller, large oblique flow angles) where separation may be present. Numerical analyses show that, while SST $k-\omega$ model does not allow for the accurate resolution of velocity field near vortical structures, it can predict adequately the location of the blade tip vortex related slipstream contraction (Krasilnikov and Sun, 2008). The simulations of propellers under heavy loading conditions done with SST $k-\omega$ model capture the changes in integral propeller characteristics when a strong flow separation on propeller blades develops.

1.3 Solution of time dependent problem

Unsteady analysis is performed in two stages. At the first stage, the solution is done using Moving Reference Frame (MRF) approach for the propeller frozen with its key blade at vertical top position, in order to provide initial conditions for time-dependent calculation. At the second stage, a time accurate solution is done with sliding mesh and with chosen time step. Temporal discretization is performed using backward differences, with implicit first-order accurate scheme. The time step chosen corresponds to propeller turn to one degree, and it is fixed during simulation. Such small time step guarantees accurate resolution of gradients in the inflow and prevents the increase in number of iterations needed for the implicit solver to converge at each time step. The maximum number of iterations per time step is set to 20. Generally, it is observed that when a periodic state in solution is approached the time step can be increased and the number of iterations per time is reduced.

3 VALIDATION EXAMPLES

The validation examples in the present paper deal with the cases of single propeller on inclined shaft and podded propeller. In the former case, the unsteadiness is caused only by crossflow, while, in the latter case, it is due to both the crossflow and interaction between propeller and pod housing. The results of formal verification of the method presented in (Krasilnikov & Sun, 2008) were used to choose adequate values of mesh factor to provide acceptable near wall resolution and achieve practical convergence at reasonable memory usage and computation time, in the simulation of shaft propellers. The calculations with single shaft propellers were carried out on ordinary office workstations with one multiple-core CPU and total 4GB RAM. For podded propellers, additional studies were required since convergence was found to be slower because of the interaction effects. These calculations required use of multiple-CPU computer clusters.

3.1 Shaft propellers in oblique flow

The first example considers the high skew, high pitch CP propeller DTMB4679 operating on inclined shaft of 7.5 degrees (crossflow from above). The geometry and test conditions for this case are available from (ITTC, 1998) along with blade surface pressure measurements due to (Jessup, 1982), and the results of numerical predictions of single blade thrust and torque by different potential codes. The LDV pressure measurements done under the two loading conditions corresponding to $J=1.078$ and $J=0.719$ (at the rate of revolution $n=8.2$ Hz) were used in the comparisons. In the RANSE computation, the mesh factor of 1.5 was used for this large propeller model ($D=0.607$ m), in order to achieve desired near wall resolution. The number of cells in the whole computation domain amounted approximately 2.86 million. Nine complete propeller revolutions were simulated at the unsteady RANSE stage to ensure converged periodic results. The convergence of propeller thrust coefficient with time iterations is illustrated in Figures 5 and 6. In general, heavier loading and larger oblique flow angle require larger number of time iterations to achieve convergence. Changes in mesh fineness do not seem to have significant effect on convergence with time iterations. The Table A1 in the Appendix 1 summarizes the results of force prediction on this propeller at lighter loading, $J=1.078$. Already the first, quasi-steady stage solution appears to be sufficient for the prediction of total propeller forces. However, it can be seen from Figures 5 and 6 that the difference between quasi-steady and converged unsteady results increases with increase of loading. However, in terms of one blade forces, the quasi-steady stage results are incorrect since the time history is not accounted for. In the considered case, when the crossflow comes onto propeller from above, the maximum blade loading corresponds to the position where blade faces the crossflow. Of the three considered blade positions (0, 120 and 240 degrees) this is 240 degrees. Quasi-steady calculation indicates maximum blade thrust at the position 0 degree. The complete unsteady calculation shows a correct load distribution between the blades with the largest thrust values at the position 240 degrees, and

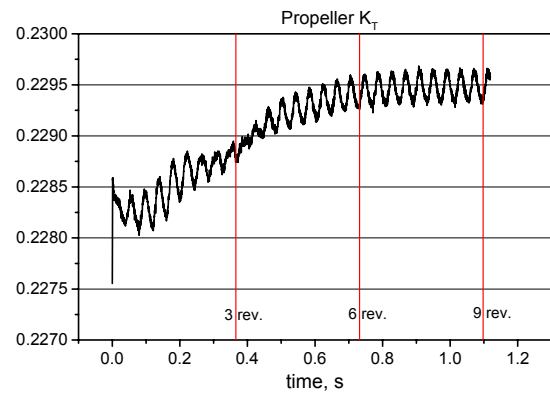


Figure 5. Convergence of propeller thrust coefficient with time iterations. Propeller DTMB4679, oblique flow angle 7.5 deg., $J=1.078$.

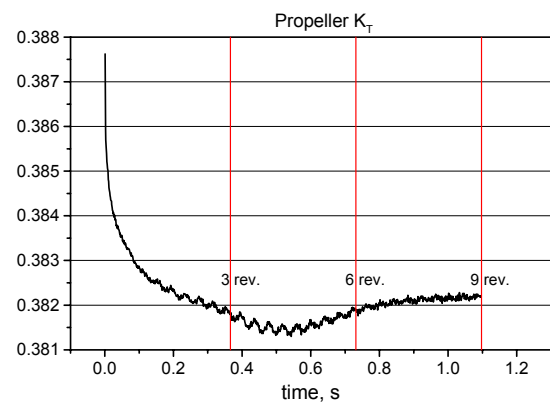


Figure 6. Convergence of propeller thrust coefficient with time iterations. Propeller DTMB4679, oblique flow angle 7.5 deg., $J=0.719$.

the smallest values at the position 120 degrees. Mesh refinement by changing the mesh factor from 2.0 to 1.5 leads to only minor change in predicted force values. Three complete propeller revolutions in unsteady simulation already bring realistic one blade force values, while strict convergence is not yet reached.

The comparison of calculated single blade thrust and torque as functions of blade position is presented in Figure 7. The present RANS results are compared with the results obtained by different panel method codes. While numerical results reveal some scatter caused, apparently, by different surface paneling, vortex wake models and methods to account for viscosity effects, it can be concluded that the unsteady RANS calculation shows tendencies close to potential code predictions. In particular, the present results appear to be close to the predictions by MARINTEK panel method code AKPA. Blade surface pressure predictions were examined for the two tested advance coefficients, at the blade positions 0, 120 and 240 degrees, and for the three cylindrical sections 0.5R, 0.7R and 0.9R. The comparisons with available LDV measurements are given in Figures 8, 9 and 10. As above, the results of AKPA panel method predictions are included.

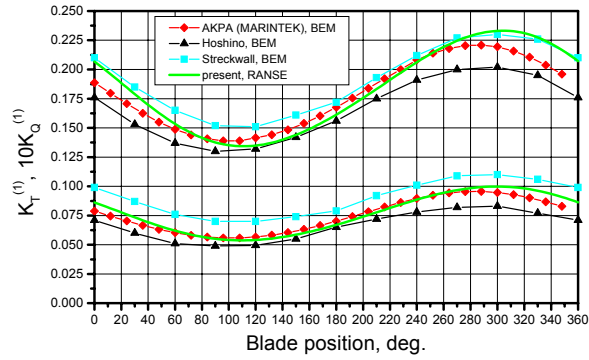


Figure 7. Predicted single blade thrust and torque coefficients as functions of blade position for the propeller DTMB4679 in oblique flow of 7.5 degrees at $J=1.078$.

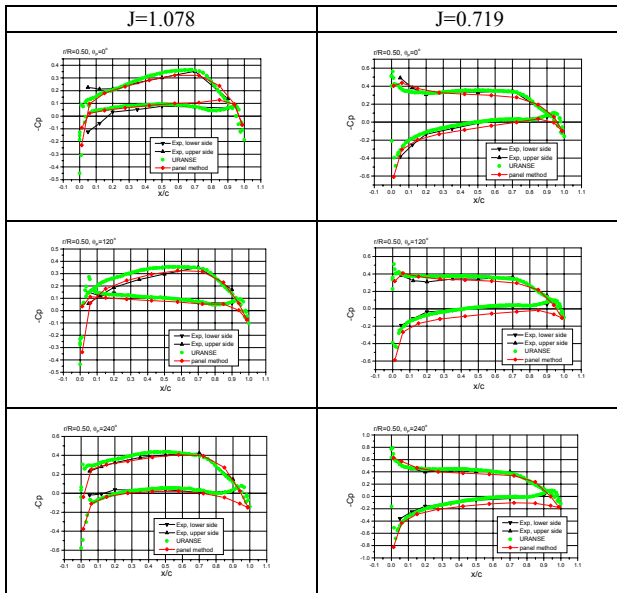


Figure 8. Measured and calculated pressure distributions on propeller DTMB4679 in oblique flow of 7.5 degrees. Blade radius $r/R=0.5$.

A satisfactory agreement is achieved for both loading conditions, and with the present RANS method it is better for heavier loading ($J=0.719$). Under lighter loading ($J=1.078$) where the relative contribution of viscosity effects is larger, the RANS calculation overpredicts negative pressure on the suction side of the blade. The reasons for that can, possibly, lie in insufficiently accurate resolution of the boundary layer on the complex surface of this high skew, high pitch blade with present mesh. Enhanced wall treatment should be attempted to evaluate the importance of boundary layer resolution. At the radius $0.9R$ the differences between numerical predictions and experimental data are the largest, which can also be attributed to boundary layer flow. In this region, the flow is influenced by 3D fluxes to a larger degree than in the inner blade region, where streamlines follow approximately cylindrical sections. On the other hand, the number of experimental points at the radius $0.9R$ is

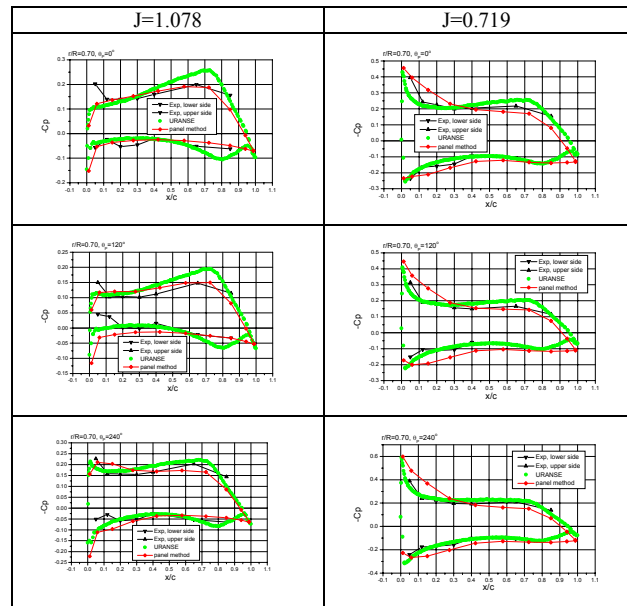


Figure 9. Measured and calculated pressure distributions on propeller DTMB4679 in oblique flow of 7.5 degrees. Blade radius $r/R=0.7$.

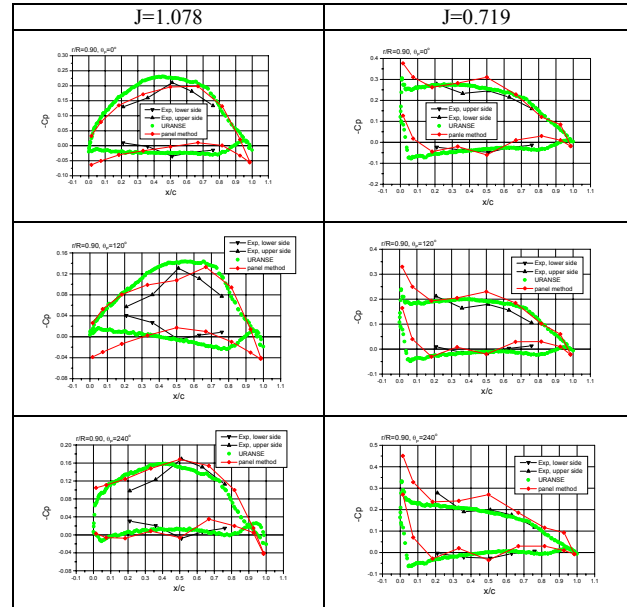


Figure 10. Measured and calculated pressure distributions on propeller DTMB4679 in oblique flow of 7.5 degrees. Blade radius $r/R=0.9$.

limited, and the accuracy of the measurements may be lower.

The second example was focused on the analysis of propeller from the tests at KMW Marine Laboratories, Kristinehamn, Sweden done for DNV in 1973 (Ræstad, 2007). The test condition corresponding to shaft inclination of 10 degrees was chosen. Propeller geometry and experimental force measurements were provided by DNV. The RANS calculations were carried out with the mesh factor of 2.0, and the comparisons were done in terms of one blade thrust, torque, transverse force and bending moment. The comparative results are presented in Figures 11, 12, 13 and 14. As above, the results obtained by panel method are given for comparison.

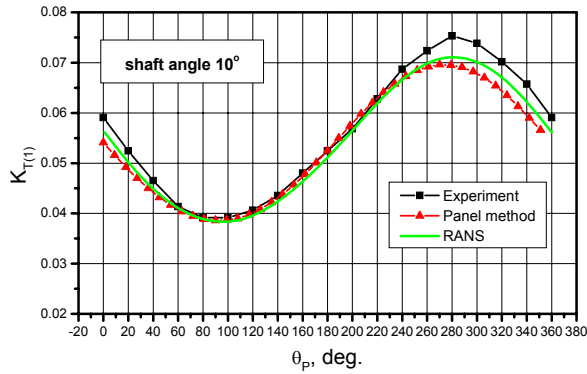


Figure 11. Measured and calculated one blade thrust vs. blade position of the propeller used in KMW/DNV tests (1973) in oblique flow of 10 degrees at $J=0.709$.

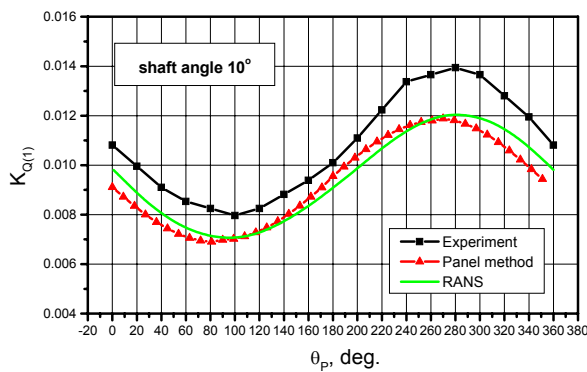


Figure 12. Measured and calculated one blade torque vs. blade position of the propeller used in KMW/DNV tests (1973) in oblique flow of 10 degrees at $J=0.709$.

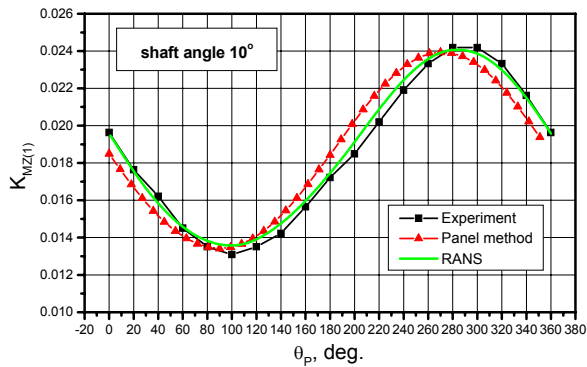


Figure 13. Measured and calculated one blade bending moment vs. blade position of the propeller used in KMW/DNV tests (1973) in oblique flow of 10 degrees at $J=0.709$.

For one blade thrust and bending moment, the results of RANS analysis are in very good agreement with experimental data and panel method prediction. The phase of these characteristics predicted by RANS is closer to that of measured data, in particular, for bending moment. The predicted values of one blade torque and transverse

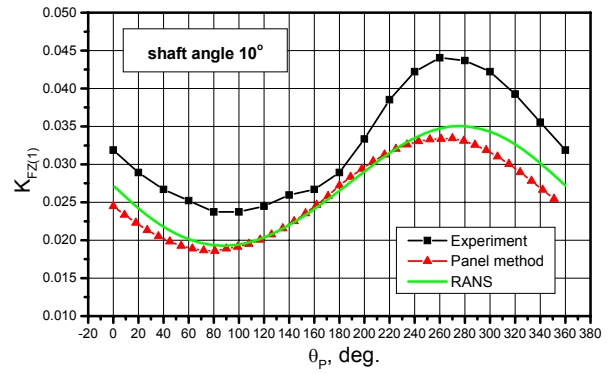


Figure 14. Measured and calculated one blade transverse force vs. blade position of the propeller used in KMW/DNV tests (1973) in oblique flow of 10 degrees at $J=0.709$.

force are lower than measured. RANS and panel method calculations show close levels of these characteristics. The calculated distributions of one blade torque and transverse force with blade position are similar to those measured in the tests.

3.2 Podded propellers in oblique flow

The analysis of podded propellers operating in oblique flow due to heading angle of pod drive represents a more complicated case compared to single propeller on shaft. The inflow on propeller is influenced by both the crossflow and interaction between propeller and housing. Because of the latter effect the flow field experienced by a pushing propeller is strongly non-uniform, and one can expect different effects on unsteady blade forces compared to pulling propeller. Interaction effects slow down convergence of time iterations in comparison with the case of single propeller. MARINTEK Pull/Push Azimuthing Thruster T14 whose general view can be seen in Figure 2 (for pulling mode) and whose main elements are reduced in Table 1 was simulated using completely unstructured mesh with the mesh factor of 2.0. The mesh contained about 1.85 million cells.

Table 1. Main elements of MARINTEK Pull/Push Azimuthing Thruster T14

	Pull	Push
Propeller		
Direction of rotation	Right-hand.	
Diameter, D [m]	0.22	
Number of blades, Z	4	
Blade area ratio	0.60	
Pitch ratio at $r/R=0.7$, P/D	1.10	
Gondola		
Length, L_{POD} [m]	0.428	
Max diameter/length ratio	0.2477	
Location of strut axis, X_R [m]	0.01	-0.01
Location of prop plane, X_P [m]	0.166	-0.166
Strut		
Span, L_{ST} [m]	0.140	
Relative chord length, c/L_{ST}	1.2	
Max section thickness t_0/c	0.1905	

The results of numerical prediction of propulsor characteristics in straight flow were considered in details in (Koushan & Krasilnikov, 2008). Therefore, in the present paper the focus will be made on the calculations in oblique flow conditions. These were carried out for propeller operating in both the pulling and pushing modes at the advance coefficient $J=0.5$ which represents moderate loading. From the tests the total forces acting on the unit were available along with propeller thrust and torque. Measurements and calculations were performed at the heading angles of $\pm 5, \pm 10, \pm 15, \pm 30$ and ± 45 degrees. Figures 15 and 16 present comparative results in terms of total axial force (F_x), total transverse force (F_y) and steering moment regarding strut axis (M_z) for the pulling and pushing units, respectively. The forces are given in ship fixed coordinated system, i.e. axial force acts along the direction of ship speed (V), positive forward, while side force is perpendicular to V , positive to starboard. Steering moment is positive in opposite clockwise direction when looking from above. In reverted flow calculations, positive heading angles correspond to crossflow coming from portside.

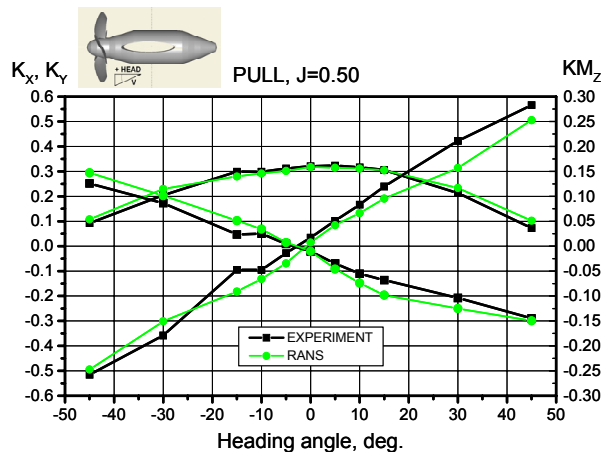


Figure 15. Prediction of total forces acting on the pulling in a range of heading angles.

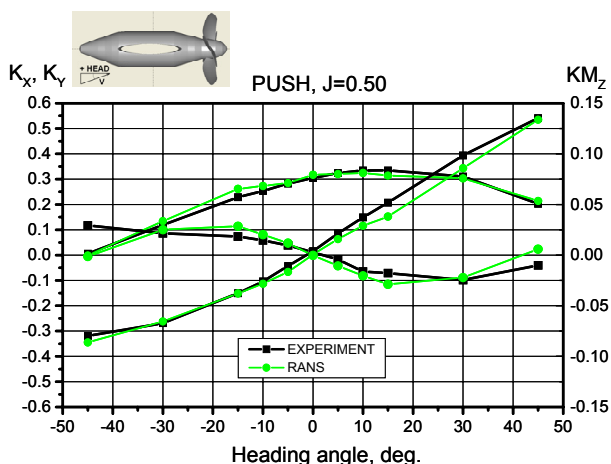


Figure 16. Prediction of total forces acting on the pushing in a range of heading angles.

From the analysis of comparative results a general conclusion can be drawn that the RANS method allows for satisfactory prediction of total forces acting on the unit in the considered range of heading angles. Axial and transverse forces are predicted close to the experimental data, with larger differences in transverse force values for the pulling unit. Larger deviations are seen for the steering moment of pushing unit at largest heading angles of ± 45 degrees where, as it will be demonstrated below, severe separation on the pod housing determines very complex interaction. The characteristics of the pulling unit are close to symmetric with respect to zero heading, while characteristics of the pushing unit reveal asymmetry which is accurately reproduced by the numerical analysis. This asymmetry is primarily due to the asymmetry in forces acting on pushing propeller, and it is caused by the interaction effects between propeller and housing. Consider the results of propeller thrust and torque predictions presented in Figure 17.

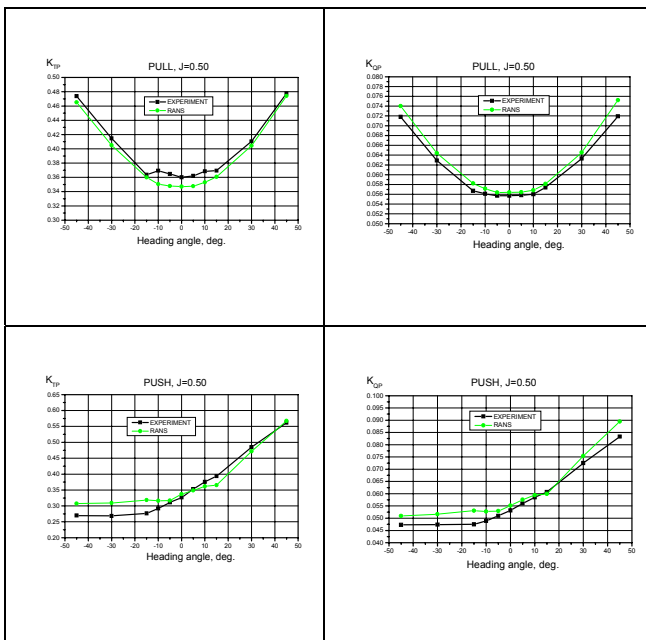


Figure 17. Prediction of thrust and torque of pulling and pushing propellers in a range of heading angles.

Thrust and torque of pulling propeller are very close to symmetric functions of heading angle. Behavior of measured thrust coefficient at smaller heading angles may be considered as indication of gap effect taking place in the tests. Thrust and torque of pushing propeller exhibit different tendencies. At positive headings, their values grow noticeably higher than those of pulling propeller. At negative heading angles, they, on the contrary, firstly, drop and then remain close to constant at heading angles large than 15 degrees. Pulling propeller experiences conditions quite similar to those of a single propeller on inclined shaft where the crossflow largely defines the dynamics of blade forces. Of course, there is some interaction with housing and, first of all, blockage effect due to strut located in the propeller slipstream, but its

effect on propeller characteristics does not change symmetry with respect to heading angle. At large heading angles, the oblique flow and propeller slipstream induce strong separation on the housing, as illustrated in Figures 18 and 19.

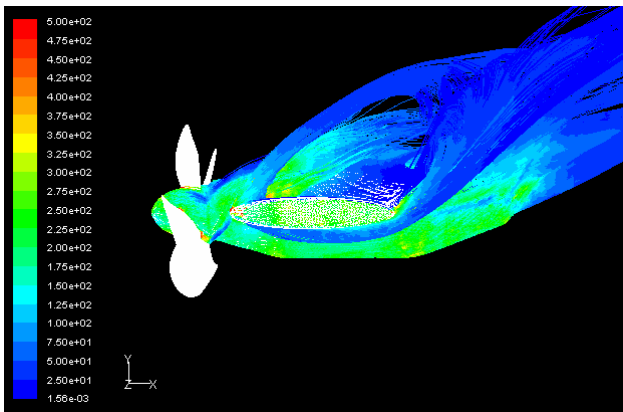


Figure 18. Streamlines released from the housing and propeller hub of the pulling propulsor operating at heading angle +30 degrees, $J=0.50$ (coloured by vorticity magnitude).

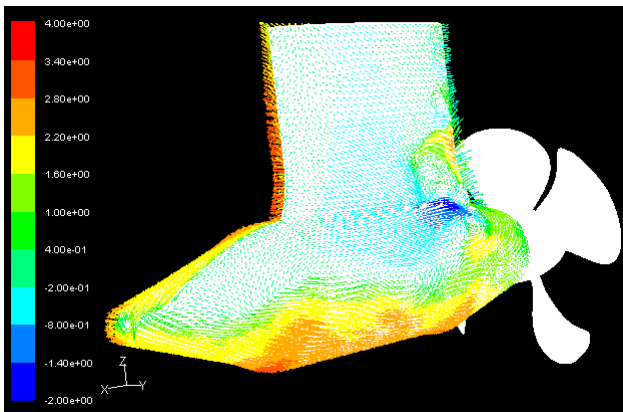


Figure 19. Velocity vectors on the housing of the pulling propulsor operating at heading angle +30 degrees, $J=0.50$ (starboard, coloured by magnitude of axial velocity).

The diagram of velocity vectors in Figure 19 indicates that reversed flow exists on almost the whole starboard side of the unit, revealing multiple zones of vorticity formation along the strut leading edge, at the strut/gondola junction and on the gondola. However, these effects seem to have minor influence on propeller characteristics. Maximum blade loading correspond to those positions where the blade encounters crossflow, i.e. bottom position (180 deg) for positive headings and top position (0 deg) for negative headings.

Unlike pulling propeller, pushing propeller interacts with both the crossflow and strut wake. At smaller heading angles, the flow around strut and gondola does not reveal strong separation, except, perhaps, local zones near strut leading and trailing edges (see Figure 20). A thin wake behind the strut, where the flow is retarded and lightly

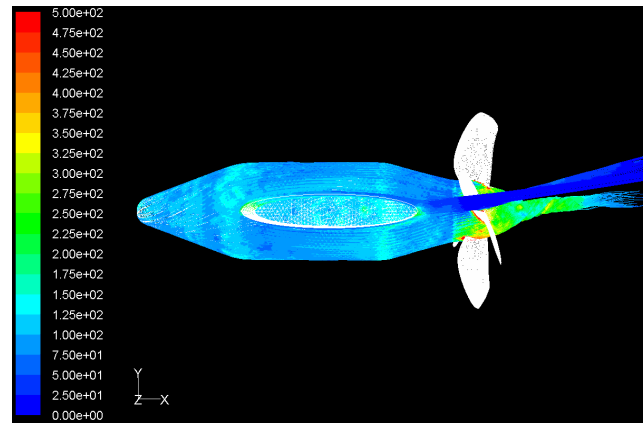


Figure 20. Streamlines released from the housing and propeller hub of the pushing propulsor operating at heading angle +10 degrees, $J=0.50$ (coloured by vorticity magnitude).

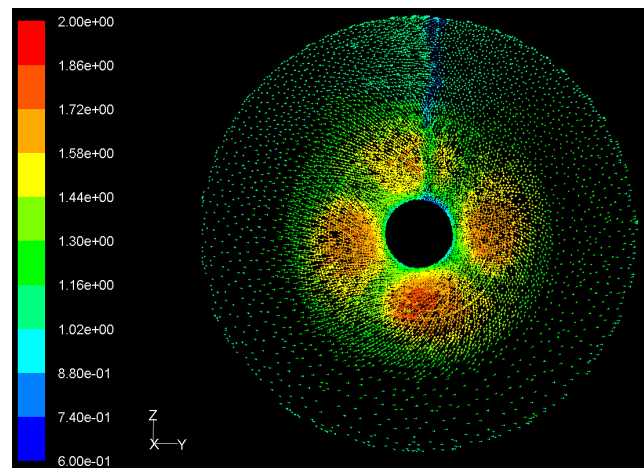


Figure 21. Velocity vectors at the section in front of pushing propeller operating at heading angle +10 degrees, $J=0.50$ (colored by magnitude of axial velocity).

swirled, but not yet reversed, is observed (see Figure 21). At larger heading angles, such as ± 30 degrees illustrated in Figures 22 – 26, a severe flow separation develops on the strut and strut/gondola junction, and, superposed with crossflow, strongly non-homogeneous inflow containing zones of swirled and reversed flows comes on propeller. With right-handed propeller, at positive heading angles, the heaviest blade loading due to crossflow occurs in the bottom part of the circle swept by propeller blades. This part is relatively undisturbed, and blade forces are comparable with those of pulling propeller. The swirled flow domain downstream of the strut, where velocity vectors are opposite to crossflow, results in increased blade loading in the upper/right part of the swept circle compared to loads on pulling propeller. As a result, pushing propeller develops larger thrust at positive headings.

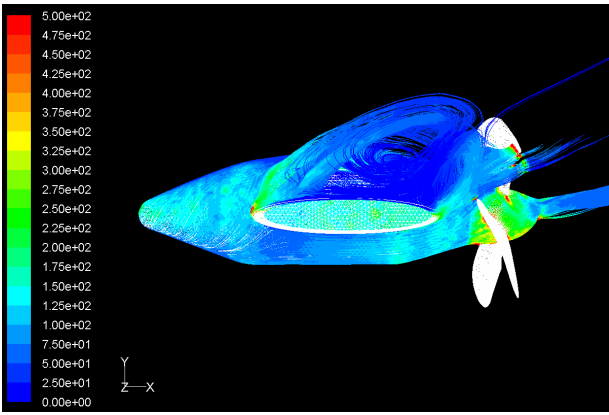


Figure 22. Streamlines released from the housing and propeller hub of the pushing propulsor operating at heading angle +30 degrees, $J=0.50$ (coloured by vorticity magnitude).

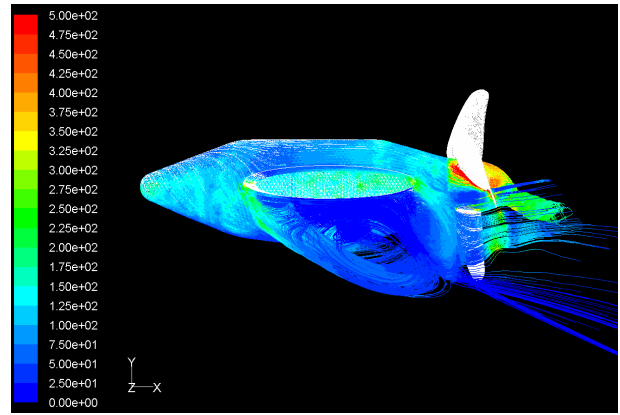


Figure 24. Streamlines released from the housing and propeller hub of the pushing propulsor operating at heading angle -30 degrees, $J=0.50$ (coloured by vorticity magnitude).

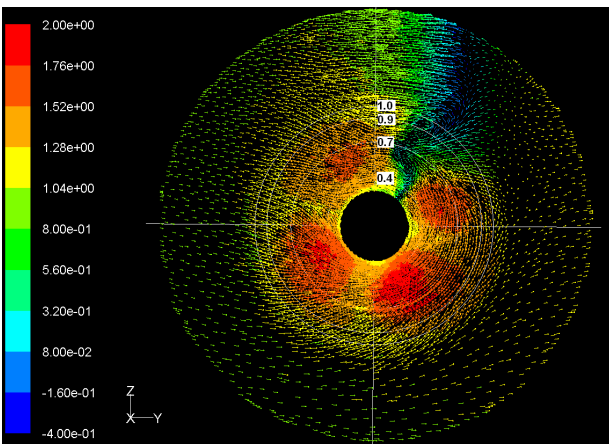


Figure 23. Velocity vectors at the section in front of pushing propeller operating at heading angle +30 degrees, $J=0.50$ (colored by magnitude of axial velocity).

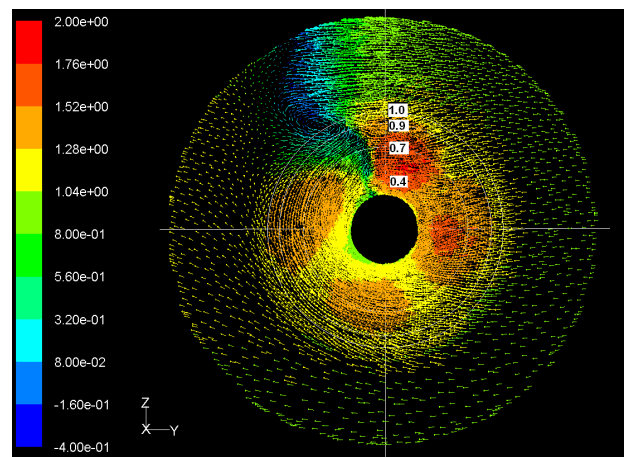


Figure 25. Velocity vectors at the section in front of pushing propeller operating at heading angle -30 degrees, $J=0.50$ (colored by magnitude of axial velocity).

However, at negative heading angles, the heaviest blade loading due to crossflow corresponds to the upper part of the swept circle where the blade interacts with separated housing wake. This interaction results in significant reduction of blade loading, which is also registered in decrease of total thrust below the level of thrust of pulling propeller.

The dynamics of one blade thrust of pulling and pushing propellers operating at the heading angles of ± 30 degrees is illustrated by the bar diagram in Figure 27. The compared values are given as related to the mean one blade thrust at zero heading. For the pulling propeller, the levels of one blade thrust and its amplitude during revolution are almost the same at positive and negative heading angles, except that maximum blade loads occur, respectively, in lower/left (180/270 deg) and upper/right (0/90 deg) parts of the swept circle. For the pushing propeller there is an apparent difference between positive and negative headings. At negative heading angles all respective blade loads are reduced, especially those corresponding to maximum loading in the upper/right (0/90 deg) part of the swept circle.

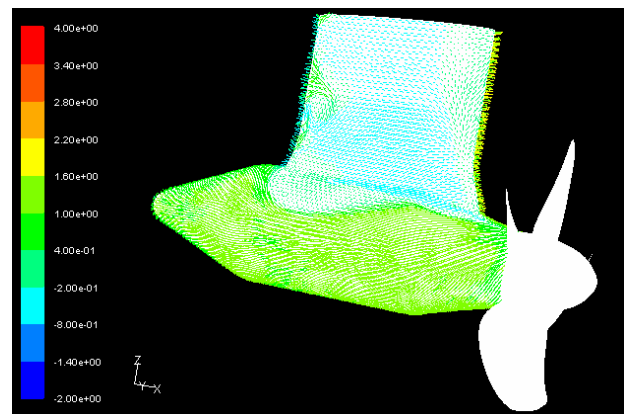


Figure 26. Velocity vectors on the housing of the pushing propulsor operating at heading angle -30 degrees, $J=0.50$ (portside, coloured by magnitude of axial velocity).

Compared to the pulling propeller, on the pushing propeller the amplitude of blade thrust is lower at negative heading angles. At positive heading angles, the blade load at the right position (90 deg) is higher than that

of pulling propeller, which is explained by its interaction with the domain of separated flow behind the strut.

As one can see from Figure 28, the amplitudes of blade loads of pushing propeller are lower at lower heading angles, which is a consequence of both the weaker crossflow and reduced strut wake.

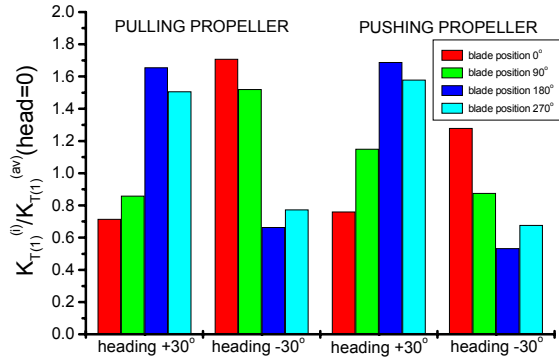


Figure 27. Dynamics of one blade thrust of pulling and pushing propellers operating at heading angles ± 30 degrees, $J=0.50$.

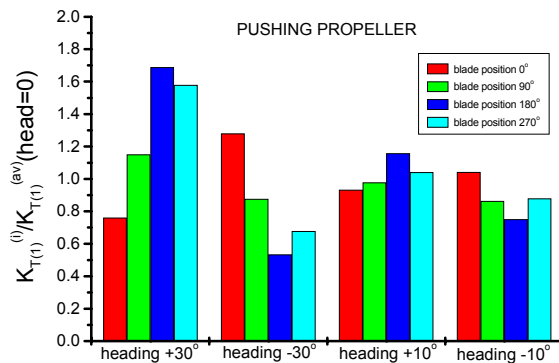


Figure 28. Dynamics of one blade thrust of pushing propeller operating at heading angles ± 30 and ± 10 degrees, $J=0.50$.

CONCLUSIONS

At present, unsteady RANS methods provide the most adequate approach to study on dynamics of unsteady blade forces. Superior to potential panel methods, they allow for simulation of propellers operating in oblique flow of larger angles including complex interactions such as take place between the components of pod propulsors. At the same time, unlike Large Eddy Simulation (LES) or Detached Eddy Simulation (DES) methods, simulations with RANS can be performed with reasonable computational resources available, or becoming more available nowadays, for engineers. Pre-processing work is greatly facilitated by the automated mesh generation tools such as used in the present work.

Validation of the employed RANS method has demonstrated its capability to predict unsteady blade forces and blade pressure distributions on propellers

operating in oblique flow with satisfactory accuracy. For podded propellers, the RANS method shows predictions of unit and propeller forces which agree well with the test data, at least in the range of heading angles from -45 to $+45$ degrees. In particular, calculations reproduce asymmetry in propeller and unit forces at positive and negative heading angles observed on pushing propulsors.

The method appears very valuable for the investigation in interaction effects between pod housing and propeller and relevant blade force dynamics. It is found by the analyses that blades of pulling propeller experience comparable amplitudes and load levels at positive and negative heading angles being mainly affected by the crossflow. The amplitudes and load levels on the blades of pushing propeller are different at positive and negative headings due to the interaction of propeller with separated strut wake. These differences increase with increase of heading angle.

Future validation work should be extended to heavier propeller loading and larger oblique flow angles which is important for the prediction of unsteady propeller and blade forces during low speed operation. Inclusion of ship hull effect in the numerical model is seen as an important task.

ACKNOWLEDGEMENT

The present research was conducted within the frameworks and with financial support of the joint industry project Norwegian Propeller Forum Phase II with the following members: Brunvoll AS, Det Norske Veritas, Finnøy Gear & Propeller AS, Heimdal Propulsion Norway AS, Helseth AS, MARINTEK, Nogva Motorfabrikk AS, Scana Volda, Servogear AS, West Mekan Produksjon AS, Wärtsilä Norway AS.

REFERENCES

- Achkinadze, A.S., Berg, A., Krasilnikov, V.I. & Stepanov, I.E. (2003). 'Numerical analysis of podded and steering systems using a velocity based source boundary element method with modified trailing edge', Proceedings of the Propellers/Shafting'2003 Symposium, Virginia Beach, VA, USA, September 17-18.
- Boswell, R., Jessup, S., & Kim, K.-H. (1981). 'Periodic single-blade loads on propellers in tangential and longitudinal wakes', SNAME Propellers'81 Symposium, Virginia Beach, VA, USA, May 26-27.
- Boswell, R., Jessup, S., Kim, K.-H., & Dahmer, D. (1984). 'Single-blade loads on propellers in inclined and axial flows', Technical report, DTNSRDC-84/084, DTNSRDC, November.
- Grygorovicz, M. & Szantyr, J.A. (2004). 'Open water experiments with two pod propulsor models', Proceeding of the First International Conference on Technological Advances in Podded Propulsion, University of Newcastle, Newcastle upon Tyne, UK, April 14-16.
- Heinke, H-J. (2004). 'Investigations about the forces and moments at podded drives', Proceeding of the First International Conference on Technological Advances in Podded Propulsion, University of Newcastle, Newcastle upon Tyne, UK, April 14-16.

- ITTC Committee. (1998). '22nd ITTC Propulsion Committee Propeller RANS/Panel Method Workshop', Grenoble, France, April 6.
- Jessup, S. (1982). 'Measurements of the pressure distribution on two model propellers', Technical report, DTNSRDC-82/035, DTNSRDC, July.
- Jessup, S. (1990). 'Measurement of multiple blade rate unsteady propeller forces', Technical report, DTRC-90/015, May.
- Junglewitz, A. & El Moctar, O.M. (2004). 'Numerical analysis of the steering capabilities of a podded drive', Ship Technology Research, Schiffstechnik, Vol.51.
- Junglewitz, A., El Moctar, O.M., & Stadie-Frohbos, G. (2004). 'Loads on podded drives', Proceedings of PRADS 2004, Luebeck, Germany.
- Koushan, K. (2006). 'Dynamics of ventilated propeller blade loading on thrusters due to forced sinusoidal heave motion', Proceedings of 26th ONR Symposium on Naval Hydrodynamics, Rome, Italy.
- Koushan, K. (2007). 'Dynamics of propeller blade and duct loadings on ventilated thrusters in dynamic positioning mode', Proceedings of Dynamic Positioning Conference, Houston, USA
- Koushan, K. & Krasilnikov, V.I. (2008). 'Experimental and numerical investigation of open thrusters in oblique flow conditions', Proceedings of the 27th ONR Symposium on Naval Hydrodynamics, Seoul, Korea, October.
- Krasilnikov V.I., Ponkratov, D.V., Achkinadze, A.S., Berg, A. & Sun, J. (2006). 'Possibilities of a viscous/potential coupled method to study scale effects on open-water characteristics of podded propulsors', Proceeding of the Second International Conference on Technological Advances in Podded Propulsion, IRENav, Brest, France, October 3-5.
- Krasilnikov, V.I., Sun, J., Zhang, Zh., & Hong, F. (2007). 'Mesh generation technique for the analysis of ducted propellers using a commercial RANSE solver and its application to scale effect study', Proceedings of the 10th Numerical Towing Tank Symposium (NuTTS'07), Hamburg, Germany, September.
- Krasilnikov, V.I. & Sun, J. (2008). 'Verification of an unsteady RANSE method for the analysis of marine propellers for high-speed crafts', Proceedings of the International Conference SuperFAST'2008, St Petersburg, Russia, July.
- Sanchez-Caja, A. & Ory, E. (2003). 'Simulation of incompressible viscous flow around a tractor thruster in model and full scale', Proceedings of the 8th International Conference on Numerical Ship Hydrodynamics, Busan, Korea.
- Sanchez-Caja, A. & Pylkkanen, J.V. (2004). 'On the hydrodynamic design of podded propulsors for fast commercial vessels', Proceedings of the TPOD2004, School of Marine Science and Technology, University of Newcastle, UK, April 14-16.
- Stanier, M. (1998). 'Investigation into propeller skew using a RANS code. Part 2: Scale effects', International Shipbuilding Progress, 45, no.443, pp.253-265.
- Ræstad, A.E. (2007). Experimental data provided for the Norwegian Propeller Forum, courtesy by DNV.
- Ukon, Y., Kudo, T., Yuasa, H., & Kamirisa, H. (1991). 'Measurement of pressure distribution on full scale propellers', Proceedings of the Propellers/Shafting'91 Symposium, SNAME, Virginia Beach, VA, USA, September.
- Zhang, Zh., Hong, F. & Tang, D. (2007). 'PreFluP – pre-processing program for the RANSE simulation of marine propulsors. Report and user's guide', CSSRC Report, December.

APPENDIX 1

Table A1. Calculated total propeller forces and single blade forces of the propeller DTMB4679 operating in oblique flow of 7.5 degrees, at J=1.078

Total propeller forces at key blade position 0°										
		Quasi-steady, m.f. 2.0			Unsteady, m.f. 2.0			Unsteady, m.f. 1.5		
KT	3	0.2273			0.2289			0.2284		
KQ	Rev.	0.05396			0.05463			0.05489		
KT	6				0.2295			0.2290		
KQ	Rev.				0.05455			0.05480		
Single blade forces										
		Quasi-steady, m.f. 2.0			Unsteady, m.f. 2.0			Unsteady, m.f. 1.5		
		0°	120°	240°	0°	120°	240°	0°	120°	240°
KT	3	0.09890	0.04484	0.08357	0.08562	0.05527	0.08803	0.08598	0.05452	0.08790
KQ	Rev.	0.02458	0.01075	0.01864	0.02044	0.01364	0.02055	0.02063	0.01359	0.02067
KT	6				0.08570	0.05481	0.08900	0.08633	0.05407	0.08862
KQ	Rev.				0.02046	0.01354	0.02054	0.02071	0.01348	0.02062